HOKKAIDO UNIVERSITY

Title	Unusually Large Thermopower Change from +330 to -185 mu V K-1 of Brownmillerite SrCoO2.5
Author(s)	Yang, Qian; Lee, Joonhyuk; Feng, Bin et al.
Citation	ACS Applied Electronic Materials, 2(7), 2250-2256 https://doi.org/10.1021/acsaelm.0c00427
Issue Date	2020-07-28
Doc URL	https://hdl.handle.net/2115/82293
Rights	This document is the Accepted Manuscript version of a Published Work that appeared in final form in ACS Applied Electronic Materials, copyright © American Chemical Society after peer review and technical editing by the publisher. To access the final edited and published work see https://pubs.acs.org/doi/10.1021/acsaelm.0c00427 .
Type	journal article
File Information	Revised Manuscript ACS Appl. Electron. Mater._clean.pdf

Hokkaido University Collection of Scholarly and Academic Papers : HUSCAP

Unusually large thermopower change from +330 μV K^{-1} to −185 μV K^{-1} of brownmillerite $SrCoO_{2.5}$

Qian Yang, Joonhyuk Lee, Bin Feng, Yuichi Ikuhara, Gowoon Kim, Hai Jun Cho, Hyoungjeen Jeen,* and Hiromichi Ohta*

Keywords

thermopower, brownmillerite $SrCoO_{2.5}$, epitaxial film, pulsed laser deposition, electronic structure

ABSTRACT: Strontium cobalt oxide ($SrCoO_{2.5}$) has recently attracted increasing attention as their optoelectronic and magnetic properties can be widely controlled using electrochemical oxidation/protonation at room temperature in air. To utilize the versatile properties of $SrCoO_{2.5}$, it is essential to evaluate the location of the Fermi energy (E_F) in the electronic structure, which is sensitive to the oxidation state of the Co ions. Here we show that the thermopower is an excellent measure for analyzing the E_F in $SrCoO_{2.5}$ epitaxial films. The lattice mismatch caused grain size reduction, which induced a slight increase in the oxidation state of the Co ions due to additional adsorbed oxygen. Although X-ray spectroscopy analyses revealed the difference of the oxidation state of the Co ions among the samples are small, an unusually large change in thermopower from +330 μV K^{-1} (lattice-matched) to −185 μV K^{-1} (lattice-mismatched) is observed from the samples due to shifts in the E_F to lower energy side. The present results demonstrate the excellent sensitivity of thermopower measurement for analyzing the location of E_F in the electronic structure of $SrCoO_{2.5}$ in the practically usable environment.

INTRODUCTION

Transition metal oxides (TMOs)[1-2] show a wide variety of functional properties including high-T_c superconductivity,[3] giant magnetoresistance,[4] and metal-to-insulator transition[5]. Among many TMOs, strontium cobalt oxide ($SrCoO_{2.5}$) has recently attracted increasing attention because their optoelectronic and magnetic properties can be widely controlled with electrochemical oxidation and protonation. In 2013, Jeen *et al.*[6-7] firstly demonstrated that $SrCoO_{2.5}$ (Co^{3+}, antiferromagnetic insulator) epitaxial films can be topotactically oxidized into $SrCoO_3$ (Co^{4+}, ferromagnetic metal) at relatively low temperature (200 °C) under an oxygen atmosphere (5 bar). In 2016, Katase *et al.*[8] utilized the topotactic redox reaction of $SrCoO_{2.5}$ film to fabricate an electrochemical memory device and demonstrated relatively fast electrochemical redox reaction at room temperature in air. Lu *et al.*[9] demonstrated the protonation of $SrCoO_{2.5}$ into $HSrCoO_{2.5}$ (Co^{2+}, ferromagnetic insulator). Both studies utilized changes in the oxidation state of the Co ions, which can be modulated from 2+ to 4+ using protonation and oxidation. In these works, thermopower measurement has been used as an indirect probe to observe large changes in oxidation state. To utilize the versatile properties and understand fundamental electronic structure of $SrCoO_{2.5}$, it is essential to evaluate the location of the Fermi energy (E_F) and its dependence on even fractional changes in the oxidation states.

The crystal structure of $SrCoO_{2.5}$ [Fig. 1(a)] is orthorhombic (a_o = 5.5739 Å, b_o = 5.4697 Å, c_o = 15.7450 Å, $\alpha = \beta = \gamma = 90°$)[10]. However, its crystal is often regarded as pseudo tetragonal (a_t = 3.905 Å, $c_t/2$ = 3.936 Å), and it is known that $SrCoO_{2.5}$ film can be grown on perovskite ABO_3 crystals such as $SrTiO_3$ (cubic perovskite, a = 3.905 Å) and $(LaAlO_3)_{0.3}(SrAl_{0.5}Ta_{0.5}O_3)_{0.7}$ (LSAT, a = 3.868 Å). According to the density functional theory (DFT) calculations,[11-12] the bandgap of $SrCoO_{2.5}$ (~0.35 eV[11]) is composed of occupied Co^o (Co in octahedral CoO_6) 3d-t_{2g} – O 2p hybridized valence band and unoccupied Co^o 3d-t_{2g} conduction band. Several studies indicate that the lattice strain can also significantly affect the properties of $SrCoO_{2.5}$. In 2018,

Zhao *et al*.[13] reported that the electrical properties of epitaxial $SrCoO_{2.5}$ thin films can be tuned by introducing epitaxial strain. Very recently, Song *et al*.[14] reported that brownmillerite $SrCoO_{2.5}$ films with different crystallographic orientations exhibited strongly anisotropic electrical conductivity. These reports suggest that the location of the E_F in the electronic structure of the $SrCoO_{2.5}$ films can be modulated if they are heteroepitaxially grown on ABO_3 substrates with different lattice mismatches[15] as shown in Fig. 1(b).

In this study, we analyzed the location of the E_F in the electronic structure of $SrCoO_{2.5}$ films heteroepitaxially grown on ABO_3 substrates with different lattice mismatches by measuring the thermopower (*S*). *S*-value is one of the observables that can estimate the electronic density of states (DOS) around the E_F. In the case of oxide semiconductors, the location of E_F can be monitored by measuring *S*.[16-18] The *S*-value can be expressed by the Mott equation,[19]

$$S = \frac{\pi^2}{3}\frac{{k_B}^2 T}{e}\left\{\frac{d[\ln(\sigma(E))]}{dE}\right\}_{E=E_F} = \frac{\pi^2}{3}\frac{{k_B}^2 T}{e}\left\{\frac{1}{n}\cdot\frac{dn(E)}{dE}+\frac{1}{\mu}\cdot\frac{d\mu(E)}{dE}\right\}_{E=E_F}$$

where k_B, e, n, and μ are the Boltzmann constant, electron charge, carrier concentration, and carrier mobility, respectively. This equation can be simplified as the partial derivative of the DOS with respect to the energy at the E_F, $\left[\frac{\partial DOS(E)}{\partial E}\right]_{E=E_F}$. As schematically illustrated in Figs. 1(c) and 1(d), when the E_F is located higher / lower energy side in the Co^o, observable *S* is positive / negative.

Here we show that the location of E_F and the shape of the Co^o state can be visualized by measuring the *S*-value of $SrCoO_{2.5}$ films on various lattice-mismatched substrates. We fabricated $SrCoO_{2.5}$ films on various lattice-mismatched substrates and measured the thermopower at room temperature in air. The microstructure analyses and the thermal annealing

results revealed that the lattice mismatch caused grain size reduction, which resulted in a slight increase of the oxidation state of the Co ions due to additional oxygen adsorption. Although the X-ray spectroscopy analyses revealed the difference of the oxidation state of the Co ions among the samples is small, unusually large change of the thermopower from +330 μV K^{-1} (lattice-matched $SrTiO_3$ substrate) to −185 μV K^{-1} (lattice-mismatched $YAlO_3$ substrate) was observed due to E_F shifts towards the lower energy side. The present results clearly demonstrate the excellent sensitivity of thermopower for analyzing the location of E_F in the electronic structure of $SrCoO_{2.5}$ in practically usable enviroment.

RESULTS AND DISCUSSION

The $SrCoO_{2.5}$ films were heteroepitaxially grown on several ABO_3 substrates. The film thickness was ~50 nm in all cases. After the film growth, we confirmed the heteroepitaxial growth of $SrCoO_{2.5}$ using reflection high energy electron diffraction (RHEED) and X-ray diffraction (XRD) measurements, and the crystallographic texture was mostly (001)[100] $SrCoO_{2.5}$ || (001)[100] ABO_3 [Figs. S1(a)−S1(f)]. Then, we measured X-ray reciprocal space mappings (RSMs) around 103 diffraction spot of the substrates of the resultant $SrCoO_{2.5}$ films to analyze the lattice parameters in the in-plane direction (*a*) and the out-of-plane direction (*c*) [Figs. S2(a)−S2(f)]. Diffraction spots of $SrCoO_{2.5}$ were clearly observed with the 103 spots of the substrate in all cases.

Figures 2(a) and 2(b) plot the extracted lattice parameters *a* and *c*, respectively. Only the films on $SrTiO_3$, LSAT, and $NdGaO_3$ show coherent epitaxial growth, in which the *a* lattice parameter agrees with that of the substrate. Since $SrTiO_3$ lattice is perfectly matched with $SrCoO_{2.5}$, only the films on LSAT and $NdGaO_3$ substrates exhibit compressive in-plane strain. The lattice parameters of the $SrCoO_{2.5}$ films on $DyScO_3$, $LaAlO_3$, and $YAlO_3$ were different

from the bulk single crystal values. In order to visualize the interface structures of $SrCoO_{2.5}$ on different substrates, cross-sectional high-angle annular dark-field scanning transmission electron microscopy (HAADF-STEM) observation was performed [Figs. S3(a)–S3(d)]. The atomic arrangement of the $SrCoO_{2.5}$ film grown on (001) $SrTiO_3$ is coherent with $SrTiO_3$ without any dislocations [Fig. S3(a)]. On the other hand, the $SrCoO_{2.5}$ on $YAlO_3$ is laminated on the $YAlO_3$ surface with misfit dislocations (arrows) every ~7 nm, which corresponds to the lattice mismatch (~5 %) [Fig. S3(b)]. This indicates that the lattice of $SrCoO_{2.5}$ on $YAlO_3$ was fully relaxed. Furthermore, *a*-axis orientated domains [Fig. S3(d)] with *c*-axis orientation [Fig. S3(c)] were observed in the $SrCoO_{2.5}$ film on $DyScO_3$ substrate. Despite the coexistence of two crystallographic orientations, the film/substrate interface was coherent.

Figures 2(c)–2(h) show topographic atomic force microscopy (AFM) images of the resultant $SrCoO_{2.5}$ films (2 μm × 2μm). While an atomically flat terraced and stepped surface is seen in the AFM image of the $SrCoO_{2.5}$ film on $SrTiO_3$ [Fig. 2(d)], the surface of other films shows intergranular features. The grain size of the films on $DyScO_3$ [Fig. 2(c)] is ~0.15 μm, LSAT [Fig. 2(e)] is ~0.3 μm, $NdGaO_3$ [Fig. 2(f)] is 0.1−0.3 μm, $LaAlO_3$ [Fig. 2(g)] is 0.2−0.3 μm, and $YAlO_3$ [Fig. 2(h)] is ~0.1 μm. The grain formation on LSAT, $NdGaO_3$, and $LaAlO_3$ is likely due to spiral growth of the $SrCoO_{2.5}$ domain, whereas that on $DyScO_3$ and $YAlO_3$ is due to the formation of misfit dislocations. The difference in the surface morphology is likely attributed to the difference in the initial film growth of $SrCoO_{2.5}$ due to the lattice mismatch.

Then, we measured the *S* of the $SrCoO_{2.5}$ films before (as-grown) and after thermal annealing at 300 °C in air. In order to measure *S* accurately, a large temperature difference (ΔT = 10 – 18 K) was introduced to the films (surface area: 10 mm × 10 mm), the thermos-electromotive force (TEMF) was measured with ΔT simultaneously. The *S* was obtained from the linear slope of

the ΔT – TEMF plots [Fig. S4(a) and S4(b)]. Figure 3(a) plots the change in the S of the $SrCoO_{2.5}$ films (blue symbols: as-grown, red symbols: after annealed at 300 °C in air) measured at room temperature. The S of the as grown $SrCoO_{2.5}$ film on LSAT substrate was +230 μV K^{-1}, close to previously reported value (+254 μV K^{-1}).[6-7] However, the $SrCoO_{2.5}$ films on other substrates showed different S. The S tends to decrease with decreasing the lattice parameter of the substrate. It should be noted that anomalously large change in thermopower from +330 μV K^{-1} (−69 μV K^{-1} after annealed at 300 °C in air) on $SrTiO_3$ to −185 μV K^{-1} (−348 μV K^{-1} after annealed at 300 °C in air) on $YAlO_3$ was observed. These results indicate a shift in the E_F in the valence band occurred as schematically shown in Figs. 3(b) and 3(c). Note that the carrier type of the $SrCoO_{2.5}$ film does not change though the sign of thermopower reversed. The reduction of thermopower after annealing in air indicates unidirectional changes in the curvature by the reduction of the number of electrons in Co for the films.

Here we briefly summarize these observations to discuss on the origin of anomalously large change in thermopower. Since the lattice parameters of the $SrCoO_{2.5}$ film on $SrTiO_3$ substrate matched with the bulk values, and the peak position of Co $L_{2,3}$ edge in the EELS spectra (Fig. S5) was not difference among the samples, the chemical composition of the resultant films was close to the stoichiometry. The XRD pattern of the $SrCoO_{2.5}$ films before and after 300 °C annealing is almost the same (Fig. S6), confirming the crystalline lattice did not change after the annealing. The electrical resistivity showed no clear tendency with the lattice mismatch (Fig. S7). The lattice strain effect is unlikely because the $SrCoO_{2.5}$ lattice on $LaAlO_3$ and $YAlO_3$ substrates does not depend on the lattice mismatch [Figs. 2(a) and 2(b)]. Since there is weak decreasing tendency of grain size with decreasing lattice mismatch [Figs. 2(c) − 2(h)], the specific surface area of the $SrCoO_{2.5}$ film grown on lattice-mismatched substrate would be larger than that on lattice-matched substrate. From these observations, we hypothesized as

follows: (1) The $SrCoO_{2.5}$ films grown on lattice-mismatched substrate adsorb oxygen gas due to their large specific surface area. (2) The adsorbed oxygen takes electrons away from the $SrCoO_{2.5}$ film, which corresponds oxidation of Co ions. (3) Therefore, the E_F shifts to the lower energy side. (4) The oxygen adsorption would strongly occur at 300 °C in air.

In order to verify the hypothesis (1) − (3), we analyzed the oxidation state of Co ion by X-ray photoelectron spectroscopy (XPS) and electron yield (EY) mode X-ray absorption spectroscopy (XAS) (Fig. S8). Tiny peak energy shift of both Co L_3 and L_2 edges were observed. The overall tendency shows that the peak energy increases with decreasing the lattice parameter of the substrate [Fig. S8(c)], indicating the stabilization of higher Co valence state with decreasing substrate lattice parameter.[6-7] Since the XPS and EY mode XAS measurements are sensitive to sample surface, these results indicate that the film surface tend to adsorb oxygen when the lattice parameter of the substrate is small.

Then, in order to verify the hypothesis (4), we annealed the $SrCoO_{2.5}$ films on (001) LSAT substrates at various temperatures (T_A) in air for 10 min and measured the XRD patterns, resistivity, and S at room temperature. As shown in Fig. S9, the peak position and the shape of the out-of-plane XRD pattern of the $SrCoO_{2.5}$ film did not change after the thermal annealing. Change in the resistivity was small (10 − 29 Ω cm) as listed in Table S1. Figure 3(d) plots the change in the S of the annealed $SrCoO_{2.5}$ films grown on (001) LSAT substrates at room temperature. Positive S-values were observed when the T_A was below 130 °C (region A) and above 320 °C (region C) whereas negative S values were observed when T_A was in the range from 130 – 320 °C (region B). These results indicate that the E_F shifts in the Co^o DOS upon the thermal annealing as schematically shown in Fig. 3(e). In region A, the E_F is located higher energy side of the Co^o DOS, showing positive S (~+140 μV K^{-1}). When T_A is in the range of

130 – 320 °C (region B), the E_F shifts to the lower energy side with negative *S*. When T_A is above 320 °C (region C), the E_F returns to the higher energy side. There are two critical temperatures, 130 °C and 320 °C. The former is due to oxygen adsorption after vaporization of water molecules from the surface, and latter is most likely desorption of oxygen from the surface of the $SrCoO_{2.5}$ film.[20-22]

Next, we measured the optical conductivity of the $SrCoO_{2.5}$ films by spectroscopic ellipsometry measurements to analyze the electronic structure. As shown in Fig. 4(a), several optical absorption peaks are present in $SrCoO_{2.5}$.[11, 13, 23] The bandgap (~0.35 eV) is the d–d transition from occupied Co^o to unoccupied Co^o. Another d–d transition from occupied Co^o to unoccupied Co^t is called α and α' [23] transition. The charge transfer transition from occupied O 2p to unoccupied Co^t is called β transition. The optical conductivity results are shown in Figs. 4(b) – 4(g). Three absorption peaks of α' (~1.1 eV[23]), α (~1.4 eV) and β (~2.5 eV) are seen. Since the top of the valence band is mainly composed of occupied Co^o, the E_F of $SrCoO_{2.5}$ locates around the tiny state of occupied Co^o. It should be noted that the peak area of α' increases with decreasing the lattice parameter of the substrate. This clearly indicates that the occupied Co^o state around the E_F increases with decreasing the lattice parameter of the substrate.

Finally, we would like to schematically illustrate the E_F in the electronic structure of the $SrCoO_{2.5}$ films on lattice-matched $SrTiO_3$ [Fig. 5(a)] and lattice-mismatched $YAlO_3$ [Fig. 5(b)]. A tiny state of Co^o exists at the top of the valence band. Since the DOS of Co^o is small, the E_F can be modulated in the state by the oxygen adsorption. When the E_F is located higher energy side of the Co^o state [Fig. 5(a)], we observe positive *S*. On the other hand, when the E_F is located lower energy side of the Co^o state [Fig. 5(b)], we observe negative *S*. Since the lattice mismatch largely affects the formation of misfit dislocations and the surface morphology of the resultant

$SrCoO_{2.5}$ films, the surfaces tend to adsorb oxygen and when the lattice mismatch is large. *S*-value exhibits some dependence on the lattice mismatch. The adsorbed oxygen takes electrons away from the film, and therefore, the E_F shifts to the lower energy side. Therefore, the *S* tends to decrease with decreasing the substrate lattice parameter. Although the X-ray spectroscopy analyses revealed that the difference in the oxidation state of the Co ions among the samples is small, thermopower detected this tiny difference sensitively, clearly showing that thermopower is excellent measure for analyzing the location of E_F in the electronic structure of $SrCoO_{2.5}$ in practically usable environment.

In addition, the huge changes in thermopower values by fractional changes of Co valence state, while keeping its crystal structure, can be used for gas sensor applications. Compared to commercialized SnO_2-based gas sensor (operating temperature ~400 °C), which requires an electric current application to sense the change of the electrical conductivity, $SrCoO_{2.5}$-based gas sensor (operating temperature ~300 °C) offers energy-saving because it generates a thermo-electromotive force (= voltage) spontaneously when there is a temperature difference. Further, the sensitivity of a $SrCoO_{2.5}$-based gas sensor is excellent because it changes the sign of the voltage when it senses gas. Thus, the gas sensing properties of $SrCoO_{2.5}$ films are of great value and need to be examined in near future.

CONCLUSION

In summary, we showed that the location of the Fermi energy (E_F) and the shape of the Co^o state in the electronic structure of $SrCoO_{2.5}$ films on various lattice-mismatched substrates can be visualized by measuring the thermopower. The microstructure analyses and the thermal annealing results revealed that the lattice mismatch caused the reduction of grain size, which resulted in a slight increase of the oxidation state of the Co ions due to adsorbed oxygen.

Although the X-ray spectroscopy analyses revealed the difference in the oxidation state of the Co ions among the samples is small, unusually large change of the thermopower from +330 μV K^{-1} (lattice-matched $SrTiO_3$ substrate) to −185 μV K^{-1} (lattice-mismatched $YAlO_3$ substrate) was observed due to the E_F shifting towards the lower energy side. The present results clearly demonstrate the excellent sensitivity of thermopower for analyzing the location of E_F in the electronic structure of $SrCoO_{2.5}$ in practically usable environment. In addition, the drastic changes in thermopower values by extremely small fractional changes of Co valence state, while keeping its crystal structure, has great potential in gas sensor applications.

EXPERIMENTAL PROCEDURES

Film growth and characterization. $SrCoO_{2.5}$ films were heteroepitaxially grown on (001) ABO_3 single crystal substrates by pulsed laser deposition (PLD). During the film deposition, the substrate temperature was kept at 750 °C, and the oxygen pressure was kept at 10 Pa. KrF excimer laser pulses (~2 J cm^{-2} $pulse^{-1}$, 10 Hz) were irradiated on the ceramic target. The film thickness was ~50 nm in all cases. In order to check the quality of the resultant films, we observed the reflection high energy electron diffraction (RHEED) patterns of the resultant films before the air exposure. The crystalline phase, orientation, lattice parameters, and thickness of the films were analyzed with high-resolution X-ray diffraction (Cu $K\alpha_1$, ATX-G, Rigaku Co.). Out-of-plane Bragg diffraction patterns and the rocking curves were measured at room temperature. The X-ray reciprocal space mappings (RSMs) were also performed to clarify the change in the $SrCoO_{2.5}$ lattice. X-ray reflection patterns were measured to evaluate the density and thickness. Atomic force microscopy (AFM, Nanocute, Hitachi Hi-Tech Sci. Co.) was used to observe the surface morphology and microstructure of the films. The atomic arrangement around the film and the substrate interface was further examined using scanning transmission electron microscopy (STEM, JEM-ARM200CF, JEOL Co. Ltd) operated at 200 keV. High-angle annular dark-field (HAADF) images were taken with detection angle of 68 – 280 mrad.

The electron energy loss spectra (EELS) were acquired in STEM mode by an Enfinium spectrometer (Gatan Inc). Dual range EELS for both zero-loss peak and core-loss peak were acquired simultaneously, allowing energy alignments.

Thermopower measurements. Thermopower of the resultant films was measured by the standard steady-state method. The film sample was placed on the gap (~5 mm) between two Peltier devices. By applying the forward/reverse current to each Peltier device, the temperature difference was generated in the sample. We measured the temperature difference (ΔT) and the thermos-electromotive force (ΔV) simultaneously at room temperature. The thermopower was calculated as the linear slope of the $\Delta T - \Delta V$ plot. The resistivity of the resultant films was measured by dc four-probe method with van der Pauw electrode configuration. In-Ga alloy was used as the contact electrodes.

Spectroscopic measurements of Co $L_{2,3}$. X-ray photoelectron spectroscopy (XPS) was used to analyze the valence state of Co in the resultant $SrCoO_{2.5}$ films. We used the Al Kα and flood gun to prevent charging at room temperature. All spectra were calibrated with C 1s peak at 284.8 eV.[24] We also performed X-ray absorption spectroscopy (XAS) around the Co $L_{2,3}$ edges of the films in Pohang accelerator laboratory (2A), and surface-sensitive electron yield mode was used (the penetration depth of X-ray ~10 nm).

ASSOCIATED CONTENT

Supporting Information

The Supporting Information is available free of charge via the Internet at http://pubs.acs.org.

Crystallographic characterization of the resultant $SrCoO_{2.5}$ films (as grown) (Fig. S1), X-ray reciprocal space mappings around 103 diffraction spots of the substrates (Fig. S2), Cross-

sectional HAADF-STEM images of the $SrCoO_{2.5}$ film / substrate interfaces (Fig. S3), Relationship between the thermo-electromotive force (TEMF) and the temperature difference (ΔT) of the $SrCoO_{2.5}$ films on various substrates (Fig. S4), Co $L_{2,3}$ edge for the thin film grown on different substrates (Fig. S5), Out-of-plane XRD patterns of the $SrCoO_{2.5}$ films grown on various substrates (Fig. S6), Temperature dependence of the resistivity of the $SrCoO_{2.5}$ films grown on various substrates (Fig. S7), Peak energy shift of Co L_3 edge. (a) XPS and (b) EY-mode XAS (Fig. S8), Out-of-plane XRD patterns of the $SrCoO_{2.5}$ films annealed at several temperatures in air (Fig. S9), and Representative values of the thermopower and the resistivity of the $SrCoO_{2.5}$ film annealed at several temperatures in air (Table S1).

AUTHOR INFORMATION

Corresponding Authors

Hyoungjeen Jeen

Department of Physics, Pusan National University, Geumjeong-gu, Busan 46241, Korea

ORCiD: orcid.org/0000-0003-2922-377X

E-mail: hjeen@pusan.ac.kr

Hiromichi Ohta

Research Institute for Electronic Science, Hokkaido University, N20W10, Kita, Sapporo 001−0020, Japan

ORCiD: orcid.org/0000-0001-7013-0343

E-mail: hiromichi.ohta@es.hokudai.ac.jp

Authors

Qian Yang

Graduate School of Information Science and Technology, Hokkaido University, N14W9, Kita, Sapporo 060−0814, Japan

ORCiD: orcid.org/0000-0002-1916-7025

Joonhyuk Lee

Department of Physics, Pusan National University, Geumjeong-gu, Busan 46241, Korea

ORCiD: orcid.org/ 0000-0001-6014-3319

Bin Feng

Institute of Engineering Innovation, The University of Tokyo, 2−11−16 Yayoi, Bunkyo, Tokyo 113−8656, Japan

ORCiD: orcid.org/0000-0002-4306-2979

Yuichi Ikuhara

Institute of Engineering Innovation, The University of Tokyo, 2−11−16 Yayoi, Bunkyo, Tokyo 113−8656, Japan

ORCiD: orcid.org/0000-0003-3886-005X

Gowoon Kim

Graduate School of Information Science and Technology, Hokkaido University, N14W9, Kita, Sapporo 060−0814, Japan

ORCiD: orcid.org/0000-0002-5803-839X

Hai Jun Cho

Research Institute for Electronic Science, Hokkaido University, N20W10, Kita, Sapporo 001−0020, Japan

ORCiD: orcid.org/0000-0002-8642-4183

Author Contributions

Q.Y. and H.O. performed the sample preparation and measurements. B.F. and Y.I. performed the STEM analyses. H.J.C. performed XPS analyses. J.L. and H.J.J. performed the XAS and the optical conductivity measurements. G.K. analyzed the optical conductivity. H.J. and H.O. planned and supervised the project. All authors discussed the results and commented on the manuscript.

Funding Sources

Hiromichi Ohta received funding from Grants-in-Aid of JSPS (19H05791, 17H01314, and the Korea-Japan bilateral program), the Asahi Glass Foundation and the Mitsubishi Foundation. Hyoungjeen Jeen received funding from NRF (NRF-2018K2A9A2A08000079). Bin Fen and Yuichi Ikuhara received funding from the MEXT Nanotechnology Platform (12024046). Gowoon Kim received funding from Grants-in-Aid for JSPS Fellows (2010147550) and the Asahi Glass Foundation Scholarship. Hai Jun Cho received funding from Nippon Sheet Glass Foundation for Materials Science and Engineering.

Notes

The authors declare no competing financial interests.

ACKNOWLEDGEMENTS

This research was supported by Grants-in-Aid for Innovative Areas (19H05791) from the JSPS. H.J.J and H.O. are supported by the Korea-Japan bilateral program funded from following programs of each country (NRF-2018K2A9A2A08000079 for H.J. and JSPS for H.O.). A part of this work was supported by Dynamic Alliance for Open Innovation Bridging Human,

Environment, and Materials, and by the Network Joint Research Center for Materials and Devices. A part of this work was also supported by the “Nanotechnology Platform” (12024046) of the MEXT (B.F. and Y.I.). G.K. was supported by Grants-in-Aid for JSPS Fellows (2010147550) from the JSPS and the Asahi Glass Foundation Scholarship. H.J.C. acknowledges the support from Nippon Sheet Glass Foundation for Materials Science and Engineering. H.O. was supported by Grants-in-Aid for Scientific Research A (17H01314) from the JSPS, the Asahi Glass Foundation and the Mitsubishi Foundation.

REFERENCES

(1) Cox, P. A., *Transition metal oxides*. Oxford University Press: New York, 1992.

(2) Hwang, H. Y.; Iwasa, Y.; Kawasaki, M.; Keimer, B.; Nagaosa, N.; Tokura, Y., Emergent phenomena at oxide interfaces. *Nat. Mater.* **2012,** *11* (2), 103-113.

(3) Wu, M. K.; Ashburn, J. R.; Torng, C. J.; Hor, P. H.; Meng, R. L.; Gao, L.; Huang, Z. J.; Wang, Y. Q.; Chu, C. W., Superconductivity at 93 K in a new mixed-phase Y-Ba-Cu-O compound system at ambient pressure. *Phys. Rev. Lett.* **1987,** *58* (9), 908-910.

(4) Jin, S.; Tiefel, T. H.; Mccormack, M.; Fastnacht, R. A.; Ramesh, R.; Chen, L. H., Thousandfold change in resistivity in magnetoresistive La-Ca-Mn-O Films. *Science* **1994,** *264* (5157), 413-415.

(5) Imada, M.; Fujimori, A.; Tokura, Y., Metal-insulator transitions. *Rev. Mod. Phys.* **1998,** *70* (4), 1039-1263.

(6) Jeen, H.; Choi, W. S.; Biegalski, M. D.; Folkman, C. M.; Tung, I. C.; Fong, D. D.; Freeland, J. W.; Shin, D.; Ohta, H.; Chisholm, M. F.; Lee, H. N., Reversible redox reactions in an epitaxially stabilized $SrCoO_x$ oxygen sponge. *Nat. Mater.* **2013,** *12* (11), 1057.

(7) Jeen, H.; Choi, W. S.; Freeland, J. W.; Ohta, H.; Jung, C. U.; Lee, H. N., Topotactic Phase Transformation of the Brownmillerite $SrCoO_{2.5}$ to the Perovskite $SrCoO_{3-\delta}$. *Adv. Mater.* **2013,** *25* (27), 3651-3656.

(8) Katase, T.; Suzuki, Y.; Ohta, H., Reversibly Switchable Electromagnetic Device with Leakage-Free Electrolyte. *Adv. Electron. Mater.* **2016,** *2* (6), 1600044.

(9) Lu, N. P.; Zhang, P. F.; Zhang, Q. H.; Qiao, R. M.; He, Q.; Li, H. B.; Wang, Y. J.; Guo, J. W.; Zhang, D.; Duan, Z.; Li, Z. L.; Wang, M.; Yang, S. Z.; Yan, M. Z.; Arenholz, E.; Zhou, S. Y.; Yang, W. L.; Gu, L.; Nan, C. W.; Wu, J.; Tokura, Y.; Yu, P., Electric-field control of tri-state phase transformation with a selective dual-ion switch. *Nature* **2017,** *546* (7656), 124.

(10) Munoz, A.; de la Calle, C.; Alonso, J. A.; Botta, P. M.; Pardo, V.; Baldomir, D.; Rivas, J., Crystallographic and magnetic structure of $SrCoO_{2.5}$ brownmillerite: Neutron study coupled with band-structure calculations. *Phys. Rev. B* **2008,** *78* (5), 054404.

(11) Choi, W. S.; Jeen, H.; Lee, J. H.; Seo, S. S. A.; Cooper, V. R.; Rabe, K. M.; Lee, H. N., Reversal of the lattice structure in $SrCoO_x$ epitaxial thin films studied by real-time optical spectroscopy and first-principles calculations. *Phys. Rev. Lett.* **2013,** *111* (9), 097401.

(12) Pardo, V.; Botta, P. M.; Baldomir, D.; Rivas, J.; Pineiro, A.; de la Calle, C.; Alonso, J. A.; Arias, J. E., Electronic structure of the antiferromagnetic phase of $Sr_2Co_2O_5$. *Physica B: Condens. Matter.* **2008,** *403* (5-9), 1636.

(13) Zhao, J. L.; Guo, H. Z.; He, X.; Zhang, Q. H.; Gu, L.; Li, X. L.; Jin, K. J.; Yang, T. Y.; Ge, C.; Luo, Y.; He, M.; Long, Y. W.; Wang, J. O.; Qian, H. J.; Wang, C.; Lu, H. B.; Yang, G. Z.; Ibrahim, K., Manipulating the structural and electronic properties of epitaxial $SrCoO_{2.5}$ thin films by tuning the epitaxial strain. *ACS Appl. Mater. Interfaces* **2018,** *10* (12), 10211-10219.

(14) Song, J. H.; Chen, Y. S.; Zhang, H. R.; Han, F. R.; Zhang, J.; Chen, X. B.; Huang, H. L.; Zhang, J. N.; Zhang, H.; Yan, X.; Khan, T.; Qi, S. J.; Yang, Z. H.; Hu, F. X.; Shen, B. G.; Sun, J. R., Strong anisotropy and its electric tuning for brownmillerite $SrCoO_{2.5}$ films with different crystal orientations. *Phys. Rev. Materials* **2019,** *3* (4), 045801.

(15) Biswas, A.; Yang, C. H.; Ramesh, R.; Jeong, M. H., Atomically flat single terminated oxide substrate surfaces. *Prog. Surf. Sci.* **2017,** *92* (2), 117-141.

(16) Ohta, H.; Mizuno, T.; Zheng, S.; Kato, T.; Ikuhara, Y.; Abe, K.; Kumomi, H.; Nomura, K.; Hosono, H., Unusually Large Enhancement of Thermopower in an Electric Field Induced Two-Dimensional Electron Gas. *Adv Mater* **2012,** *24* (6), 740-744.

(17) Sanchela, A.; Onozato, T.; Feng, B.; Ikuhara, Y.; Ohta, H., Thermopower modulation clarification of the intrinsic effective mass in transparent oxide semiconductor $BaSnO_3$. *Phys Rev Mater* **2017,** *1* (3), 034603.

(18) Sanchela, A. V.; Wei, M.; Cho, H. J.; Ohta, H., Thermopower Modulation Clarification of the Operating Mechanism in Wide Bandgap $BaSnO_3$-$SrSnO_3$ Solid-Solution Based Thin Film Transistors. *Small* **2019,** *15* (8), 1805394.

(19) Cutler, M.; Mott, N. F., Observation of Anderson localization in an electron gas. *Phys. Rev.* **1969,** *181* (3), 1336.

(20) Higuchi, K.; Sugiyama, H.; Kubota, J., Molecular and Dissociative Adsorption of Oxygen on Solid Oxide Fuel Cell Cathode Materials of $La_{1-x}Sr_xCoO_3$, $La_{1-x}Sr_xCo_{1-y}Fe_yO_3$, and $La_{1-x}Sr_xMnO_3$ Studied by Temperature-Programmed Desorption. *J. Phys. Chem. C* **2017,** *121* (27), 14581-14588.

(21) Wang, J.; Yang, T. R.; Lei, L. B.; Huang, K., Ta-Doped $SrCoO_{3-\delta}$ as a promising bifunctional oxygen electrode for reversible solid oxide fuel cells: a focused study on stability. *J. Mater. Chem. A* **2017,** *5* (19), 8989-9002.

(22) Wang, J.; Jin, X. F.; Huang, K., A new defect chemistry model for Nb-doped $SrCoO_{2.5+\delta}$: The role of oxygen interstitials and delocalized-to-localized electron holes. *J. Solid State Chem.* **2017,** *246*, 97-106.

(23) Lee, J. H.; Choi, W. S.; Jeen, H.; Lee, H. J.; Seo, J. H.; Nam, J.; Yeom, M. S.; Lee, H. N., Strongly coupled magnetic and electronic transitions in multivalent strontium cobaltites. *Sci. Rep.* **2017,** *7*, 16066.

(24) Swift, P., Adventitious carbon—the panacea for energy referencing? *Surf. Interf. Anal.* **1982,** *4* (2), 47.

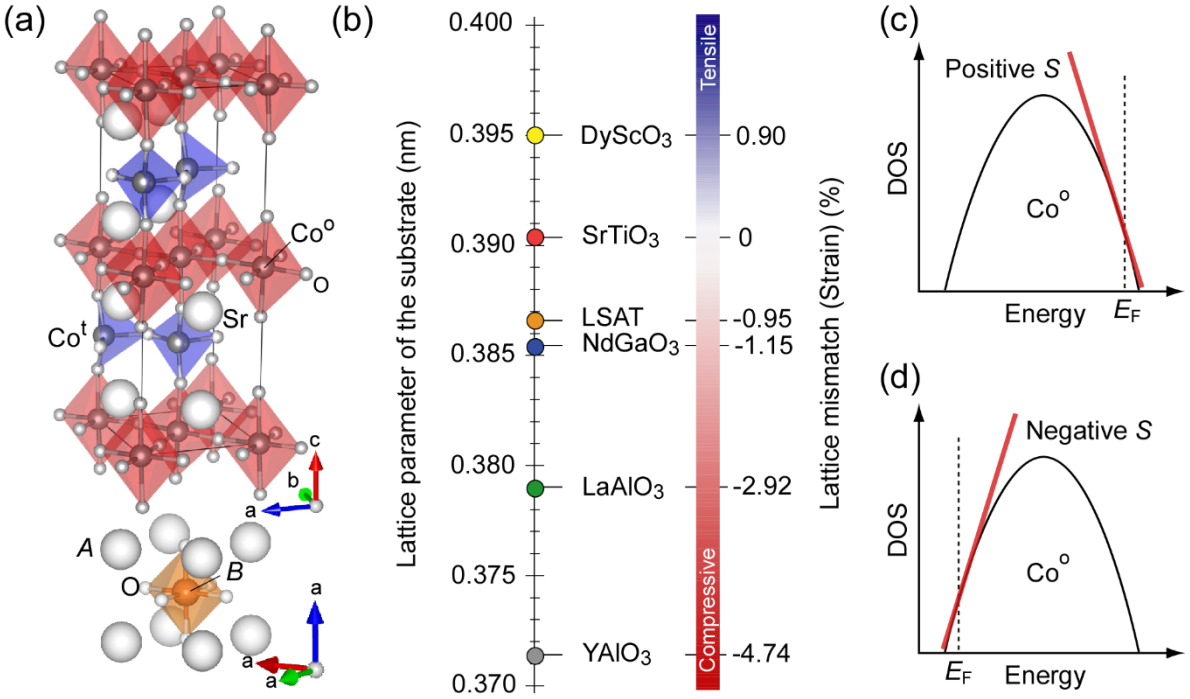

Figure 1. (a) Schematic crystal structures of brownmillerite $SrCoO_{2.5}$ film and ABO_3 perovskite substrate. Co^o and Co^t indicate Co ions in distorted CoO_6 octahedral and Co ions in distorted CoO_4 tetrahedral, respectively. (b) Relationship between the lattice parameter of the substrates and the lattice mismatch and/or lattice strain between $SrCoO_{2.5}$ film and the substrate. (c)(d) Schematic energy band diagram of the density of states (DOS) of Co^o in $SrCoO_{2.5}$ around the Fermi energy (E_F). When the E_F is located (c) higher energy side / (d) lower energy side, observable S is (c) positive / (d) negative.

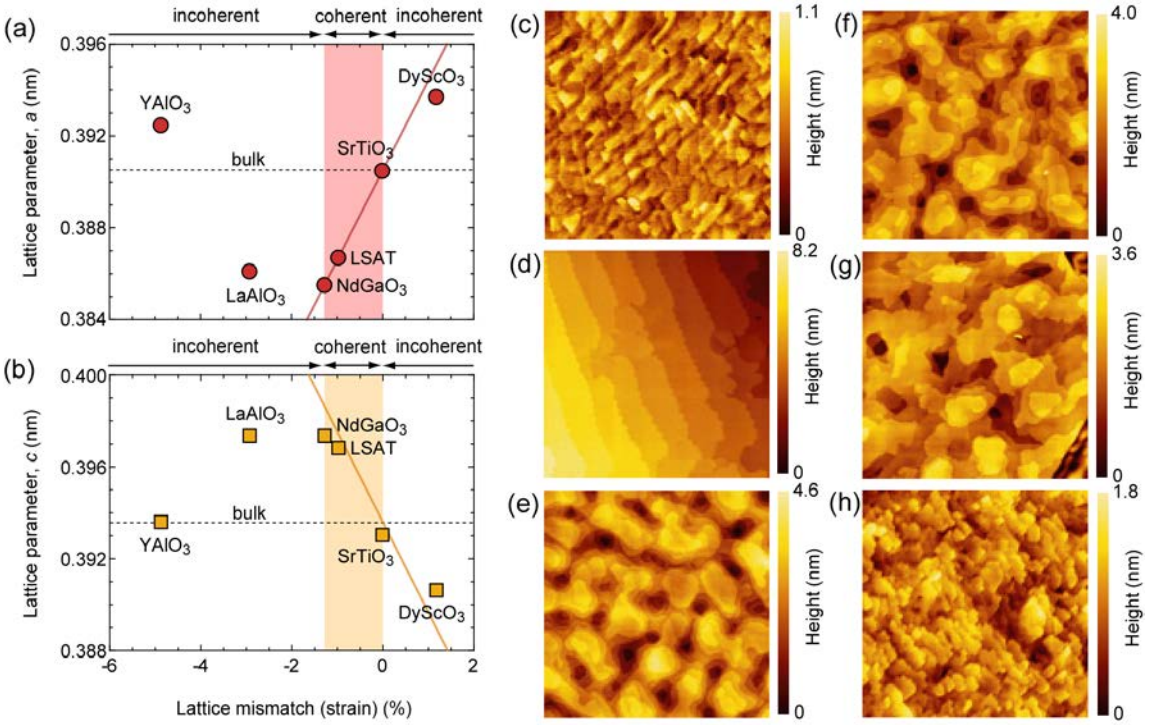

Figure 2. Lattice parameters of (a) *a* and (b) *c* for the $SrCoO_{2.5}$ films grown on lattice-mismatched substrates. Dotted lines show the bulk values. Solid lines indicate the ideal coherent growth of the film. Only the films on $SrTiO_3$, LSAT, and $NdGaO_3$ show coherent epitaxial growth. (c) – (h) Topographic AFM images (2 μm × 2μm) of the $SrCoO_{2.5}$ films grown on (c) $DyScO_3$, (d) $SrTiO_3$, (e) LSAT, (f) $NdGaO_3$, (g) $LaAlO_3$, and (h) $YAlO_3$ substrates. Atomically flat terraced and stepped surface is seen in the $SrCoO_{2.5}$ film on $SrTiO_3$. The grain size of the films on $DyScO_3$ is ~0.15 μm, on LSAT is ~0.3 μm, on $NdGaO_3$ is 0.1 − 0.3 μm, on $LaAlO_3$ is 0.2 − 0.3 μm, and on $YAlO_3$ is ~0.1 μm.

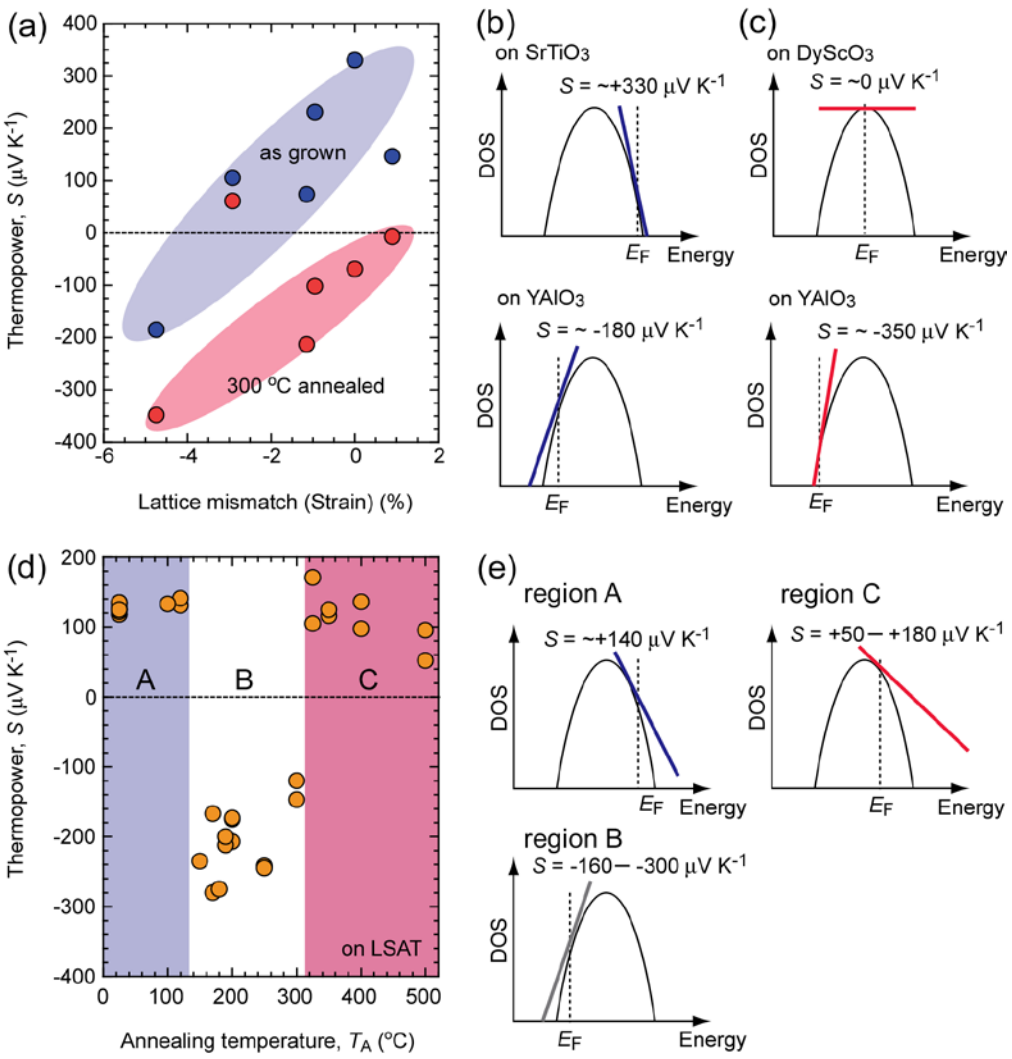

Figure 3. (a) Change in the thermopower (S) of the $SrCoO_{2.5}$ films (blue symbols: as grown, red symbols: annealed at 300 °C in air) measured at room temperature. The S tends to decrease with decreasing the lattice parameter of the substrate. The annealed films mostly showed smaller S. (b)(c) Schematic energy band diagram of the $SrCoO_{2.5}$ film around the Fermi energy (E_F) [(b) as grown and (c) after 300 °C annealing in air]. (d) Change in the S of the $SrCoO_{2.5}$ film grown on LSAT substrate after annealing at T_A in air. The S measurements were performed at room temperature. Positive S-values were observed when the T_A is below 130 °C (region **A**) and above 320 °C (region **C**) whereas negative S-values were observed when the T_A is in the range from 130 – 320 °C (region **B**). (e) Schematic energy band diagram of the $SrCoO_{2.5}$ film after annealing at the T_A region **A**, **B**, and **C**. The E_F moved upon the thermal annealing.

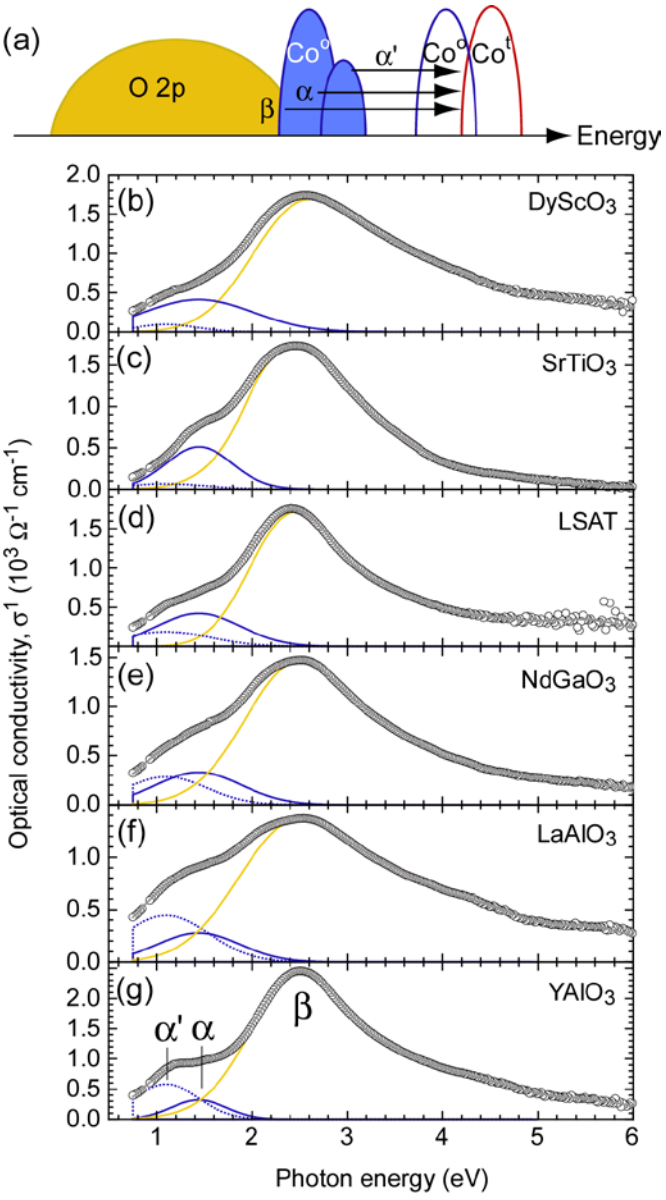

Figure 4. (a) Schematic energy band structure of $SrCoO_{2.5}$. The bandgap is ~0.35 eV, which is composed of d−d transition from Co^{o} to Co^{o}. In addition to the bandgap, optical absorptions occur at α, α' (d−d transition from Co^{o} to Co^{t}) and β (charge transfer transition from O 2p to Co^{t}). (b−g) Optical conductivity of the $SrCoO_{2.5}$ films (as-grown). The optical absorptions peaking around 1.1 eV (α'), 1.4 eV (α) and around 2.5 eV (β) are seen. Note that the peak area of α' increases with decreasing the lattice parameter of the substrate.

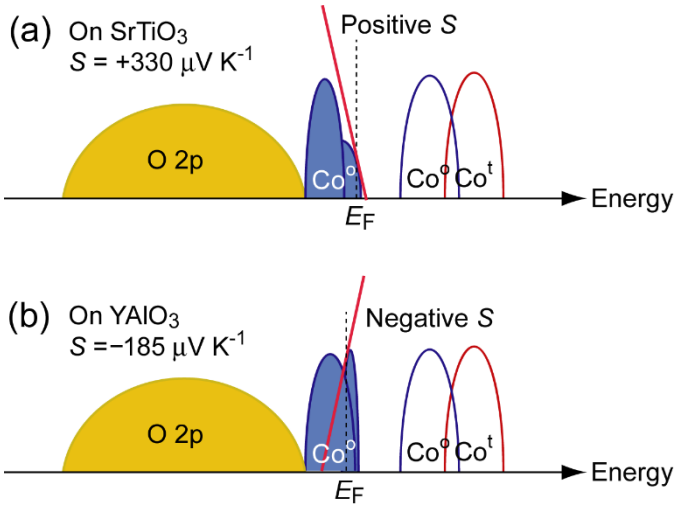

Figure 5. Schematic energy band structure of (a) $SrCoO_{2.5}$ on $SrTiO_3$ and (b) on $YAlO_3$ substrates (as-grown). The $SrCoO_{2.5}$ film on $SrTiO_3$ shows positive thermopower (*S*) whereas that on $YAlO_3$ shows negative *S*. The E_F of the $SrCoO_{2.5}$ film on (a) $SrTiO_3$ locates higher energy side of α' whereas that on (b) $YAlO_3$ locates lower energy side of α'.

Supporting Information

Unusually large thermopower change from +330 μV K^{-1} to −185 μV K^{-1} of brownmillerite $SrCoO_{2.5}$

Qian Yang[1], Joonhyuk Lee[2], Bin Feng[3], Yuichi Ikuhara[3], Gowoon Kim[1], Hai Jun Cho[1,4], Hyoungjeen Jeen*[,2], and Hiromichi Ohta*[,1,4]

[1]Graduate School of Information Science and Technology, Hokkaido University, N14W9, Kita, Sapporo 060−0814, Japan

[2]Department of Physics, Pusan National University, Geumjeong-gu, Busan 46241, Korea

[3]Institute of Engineering Innovation, The University of Tokyo, 2−11−16 Yayoi, Bunkyo, Tokyo 113−8656, Japan

[4]Research Institute for Electronic Science, Hokkaido University, N20W10, Kita, Sapporo 001−0020, Japan

***Corresponding Authors**

Hyoungjeen Jeen email: hjeen@pusan.ac.kr

Hiromichi Ohta email: hiromichi.ohta@es.hokudai.ac.jp

Keywords

thermopower, brownmillerite $SrCoO_{2.5}$, epitaxial film, pulsed laser deposition, electronic structure

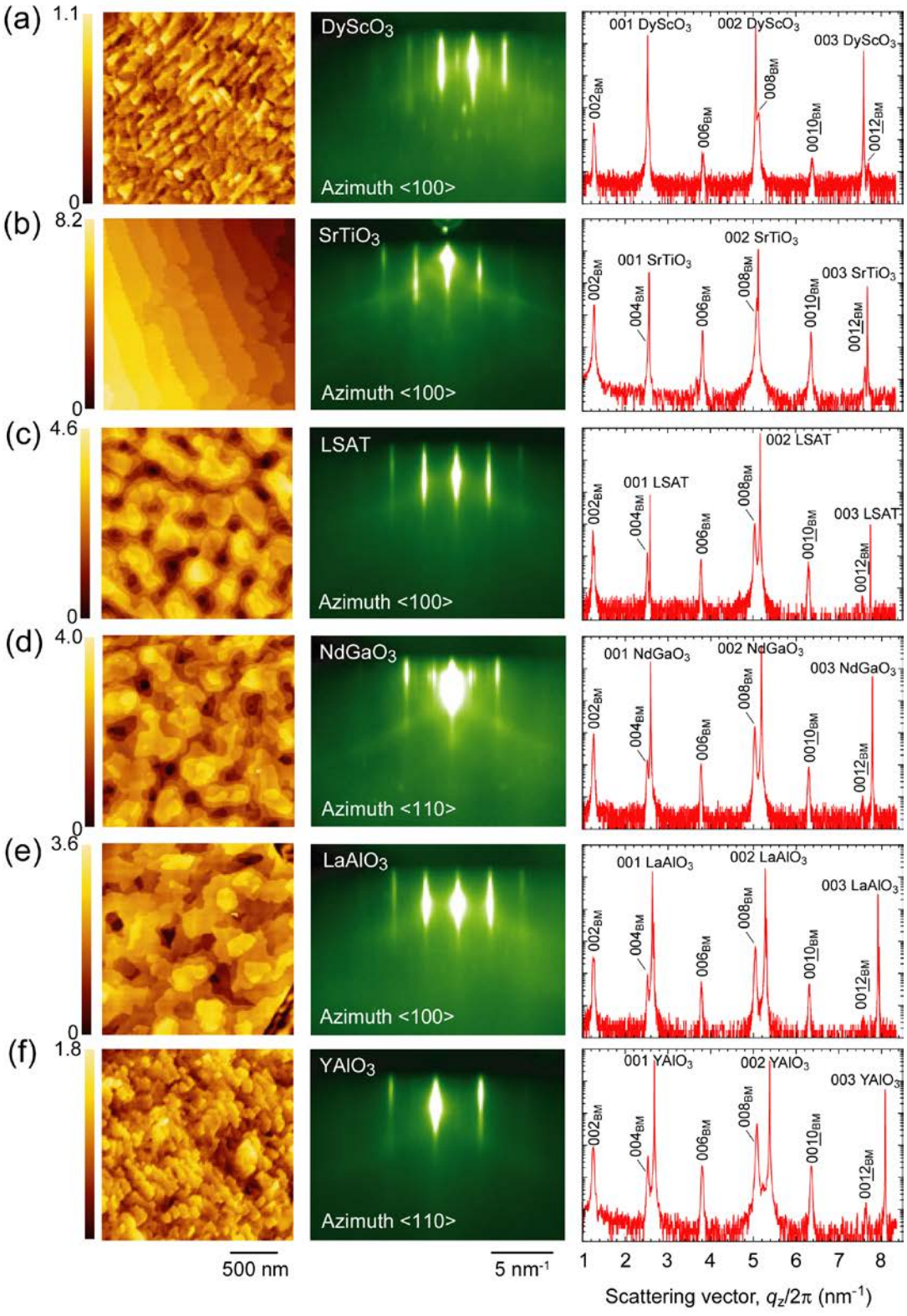

Figure S1. Crystallographic characterization of the resultant $SrCoO_{2.5}$ films (as grown). (from left to right) Topographic AFM images, RHEED patterns and out-of-plane XRD Bragg diffraction patterns of the $SrCoO_{2.5}$ films on (a) $DyScO_3$, (b) $SrTiO_3$, (c) LSAT, (d) $NdGaO_3$, (e) $LaAlO_3$, and (f) $YAlO_3$.

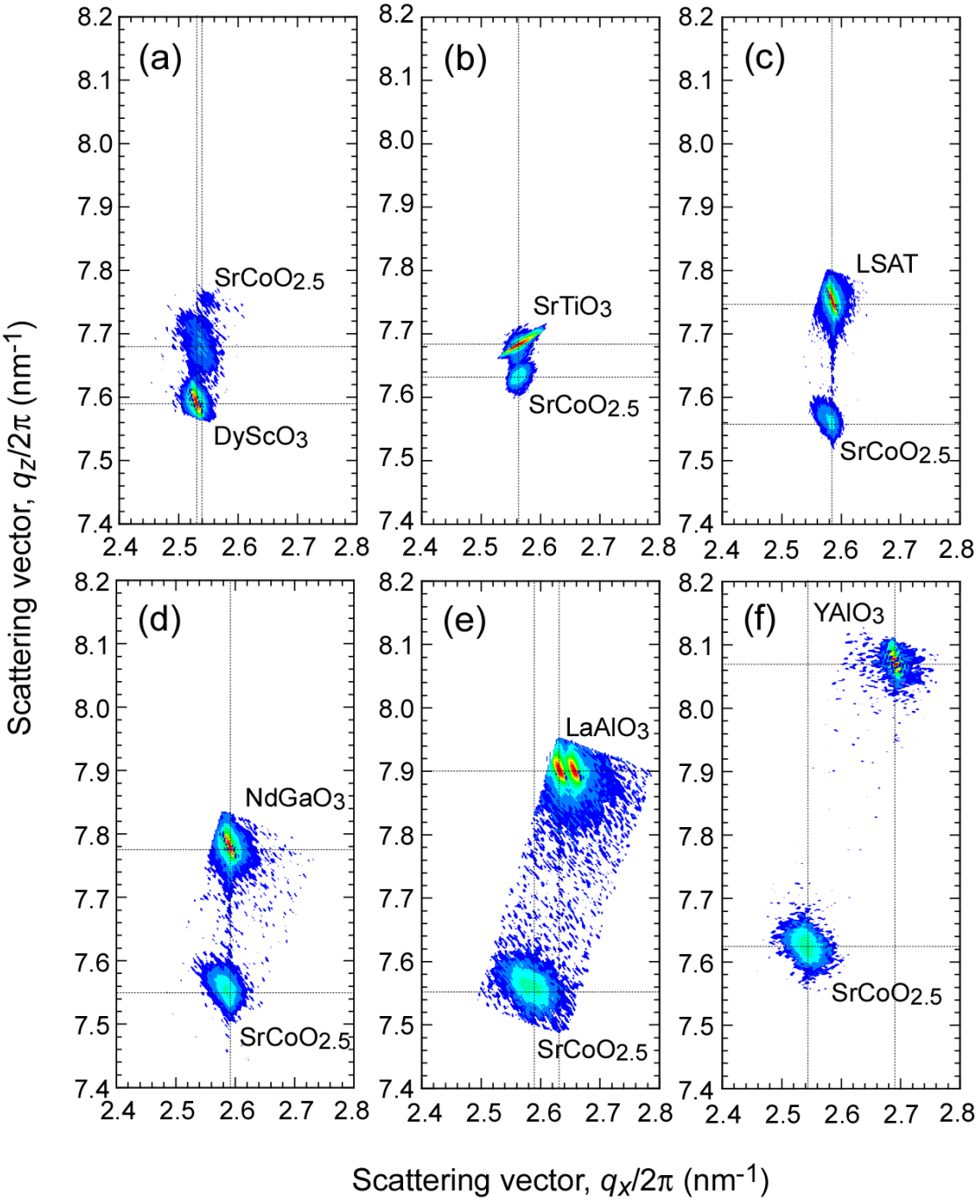

Figure S2. X-ray reciprocal space mappings around 103 diffraction spots of the substrates. The solid lines indicate the peak positions. Coherent epitaxial growth occurred only on $SrTiO_3$, LSAT, and $NdGaO_3$ substrates.

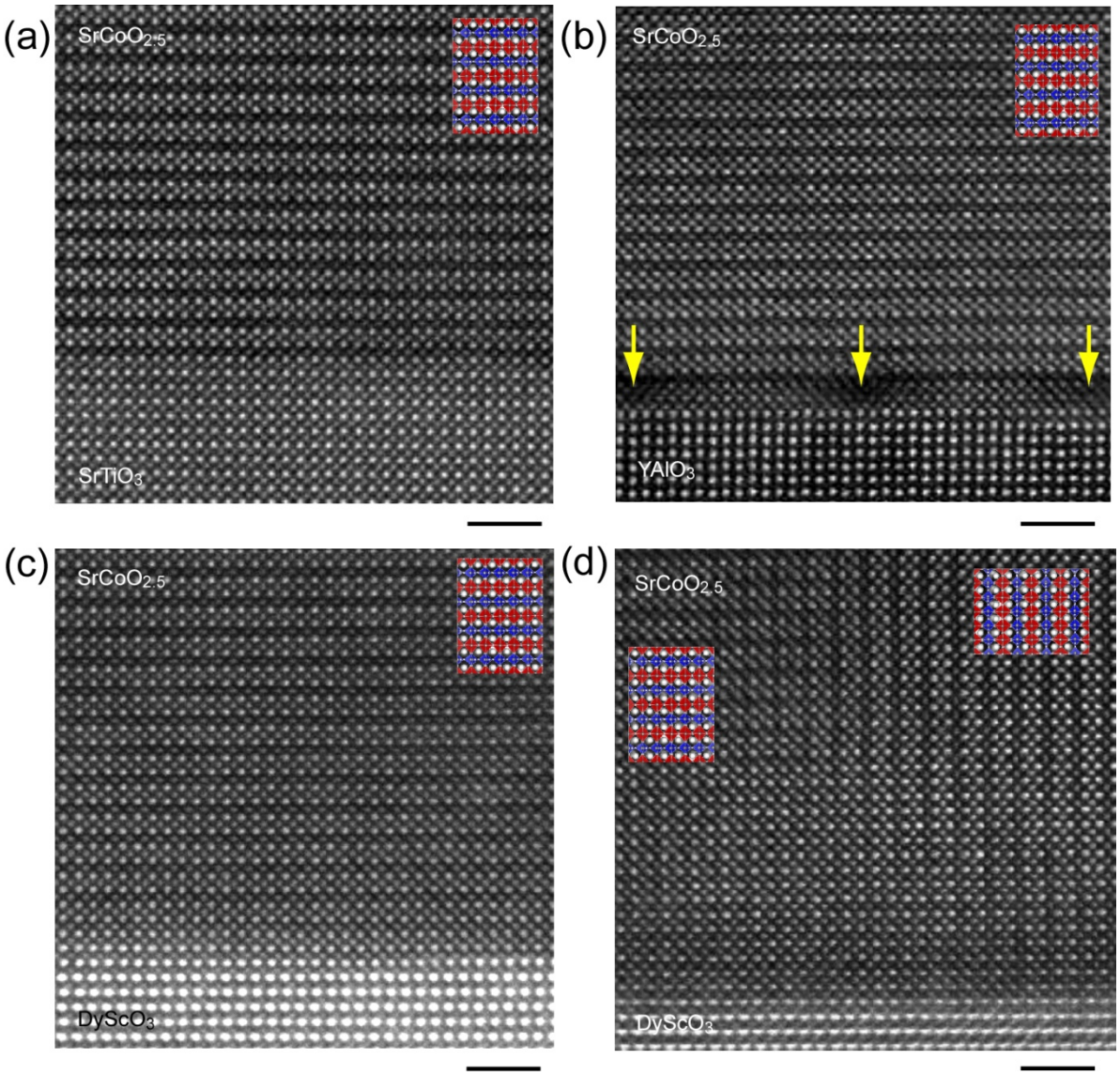

Figure S3. Cross-sectional HAADF-STEM images of the $SrCoO_{2.5}$ film / substrate interfaces on (a) $SrTiO_3$, (b) $YAlO_3$, and (c and d) $DyScO_3$ substrates. The scale bar is 2 nm. The schematic crystal structure is also shown to visualize the crystallographic orientation of the films. The arrows in (b) indicate the misfit dislocations.

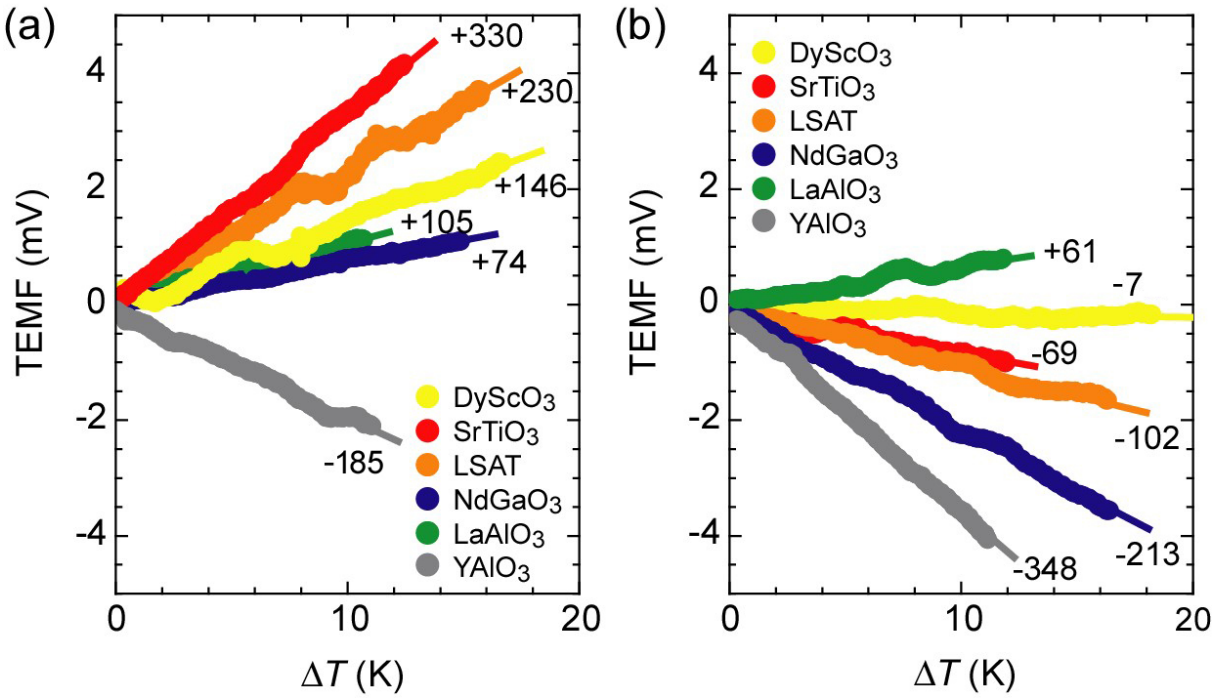

Figure S4. Relationship between the thermo-electromotive force (TEMF) and the temperature difference (ΔT) of the $SrCoO_{2.5}$ films on various substrates. (a) as grown films and (b) annealed at 300 °C in the air. The thermopower values were obtained from the slope of the plots. The unit of the thermopower values is $\mu V \cdot K^{-1}$. These measurements were performed at room temperature in air.

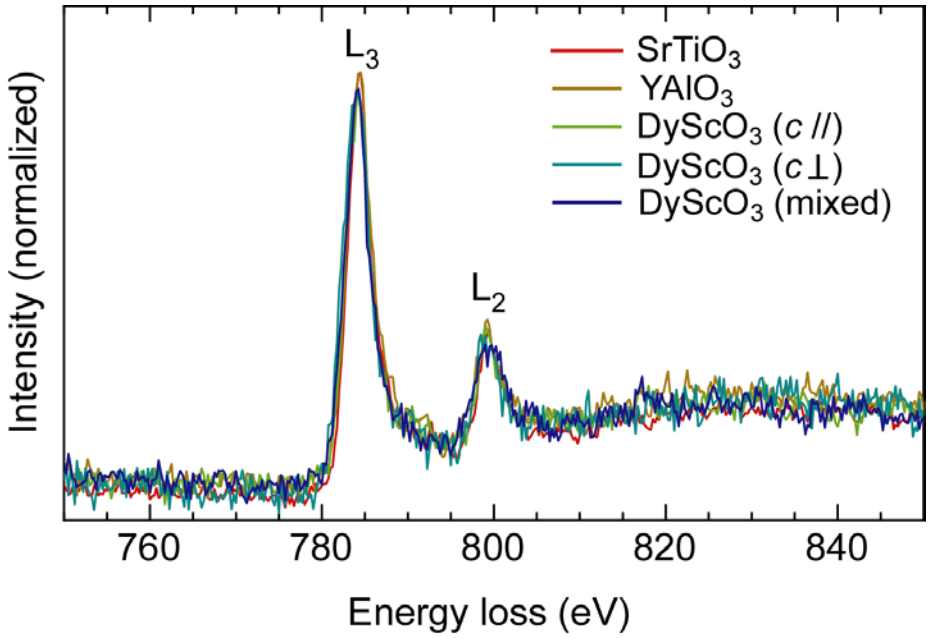

Figure S5. Co $L_{2,3}$ edge for the thin film grown on different substrates. The intensities are normalized by Co L_3 edge.

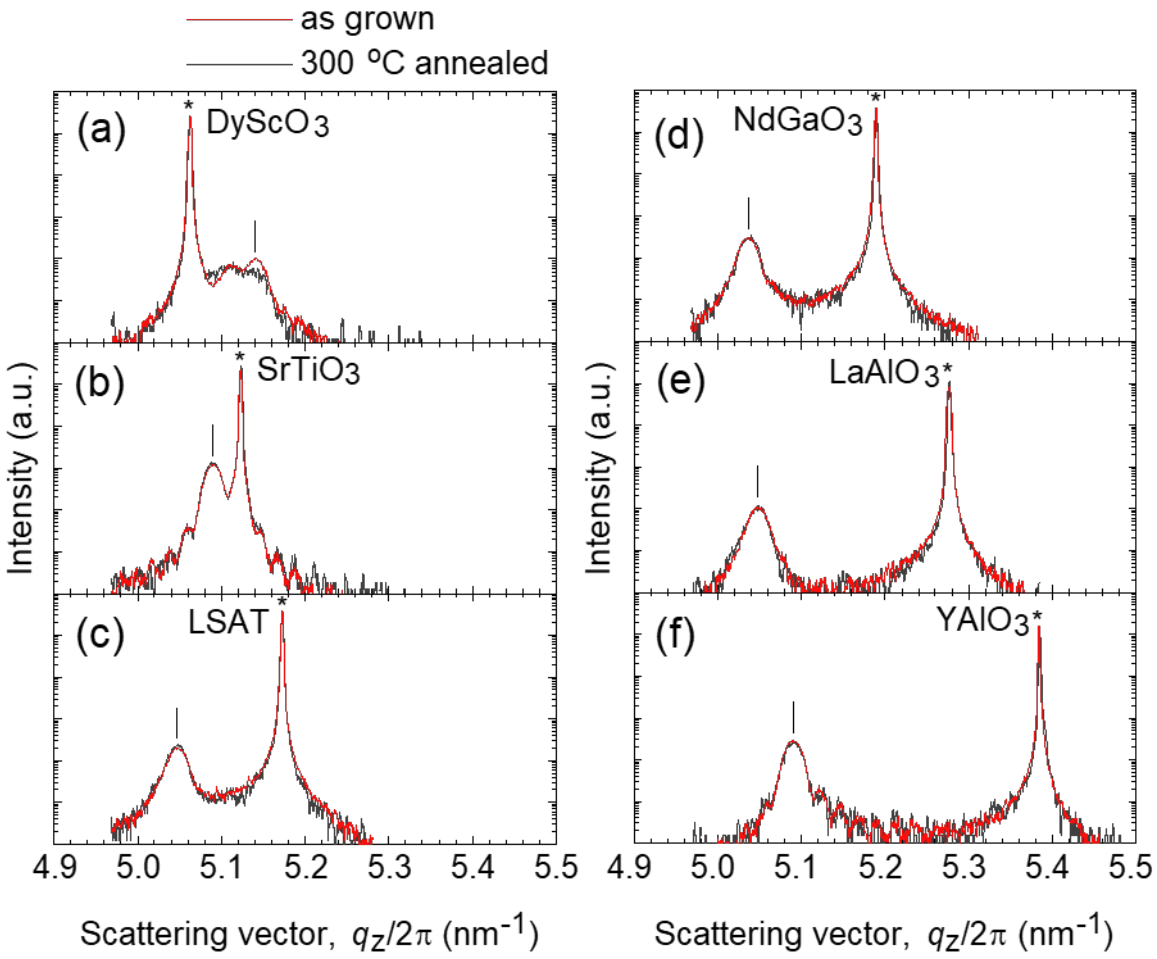

Figure S6. Out-of-plane XRD patterns of the $SrCoO_{2.5}$ films grown on various substrates (a) $DyScO_3$, (b) $SrTiO_3$, (c) LSAT, (d) $NdGaO_3$, (e) $LaAlO_3$, and (f) $YAlO_3$. The XRD pattern of the $SrCoO_{2.5}$ films before and after 300 °C annealing is almost the same, confirming the crystalline lattice did not change after the annealing.

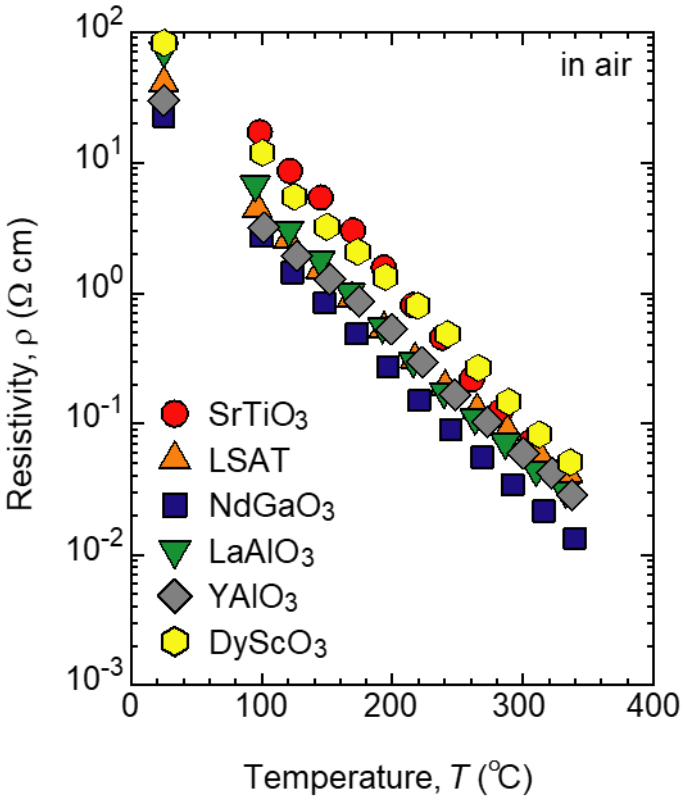

Figure S7. Temperature dependence of the resistivity of the $SrCoO_{2.5}$ films grown on various substrates. The resistivity was measured in air. The electrical resistivity showed no clear tendency with the lattice mismatch.

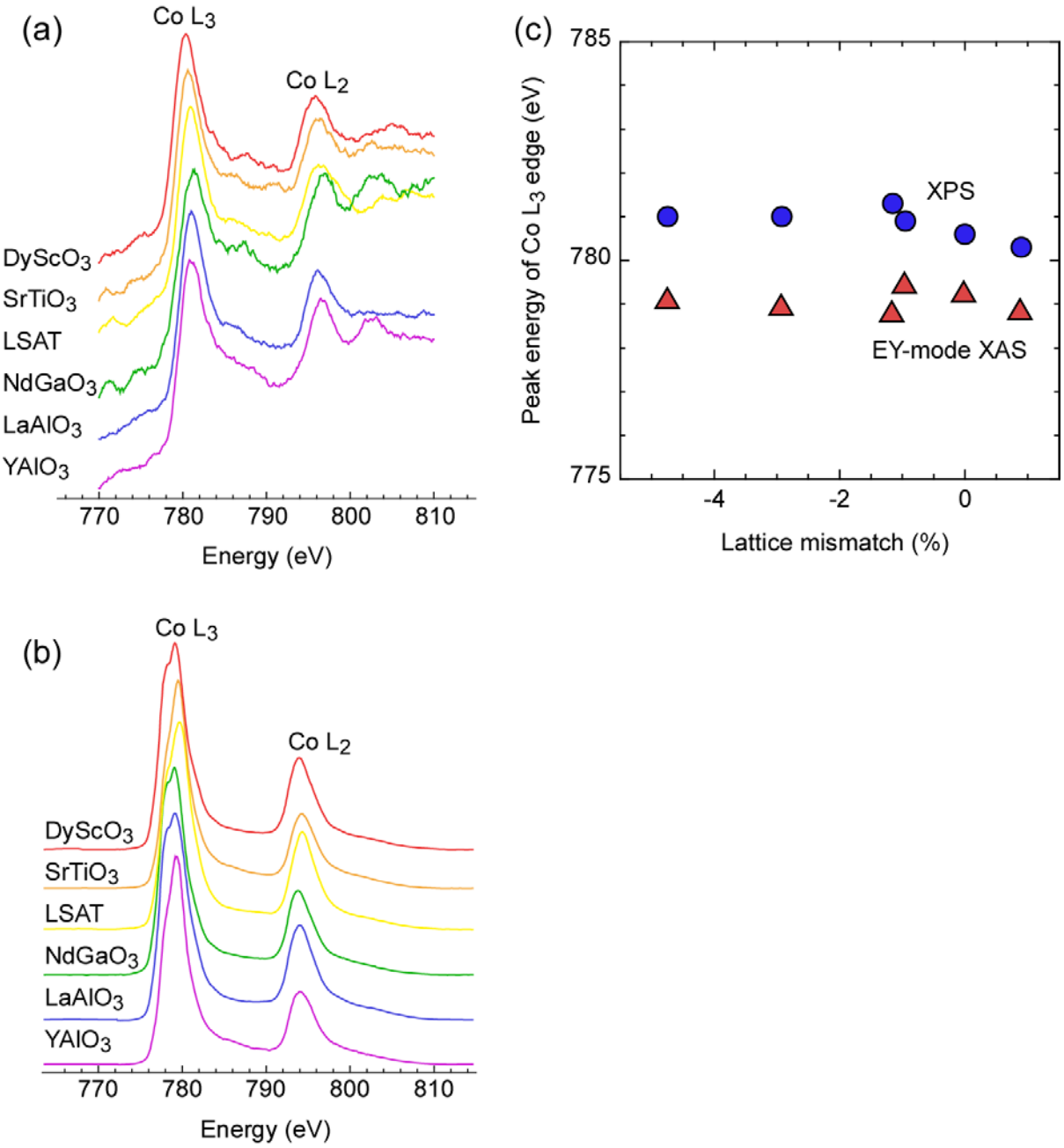

Figure S8. Peak energy shift of Co L_3 edge. (a) XPS and (b) EY-mode XAS. (c) The plot of the peak energy of Co L_3 edge as a function of the lattice mismatch. Tiny peak energy shift of both Co L_3 and L_2 edges are observed. Since the XPS and EY mode XAS measurements are sensitive to sample surface, these results indicate oxygen adsorption at the film surface tend to be occurred when the lattice parameter of the substrate is small.

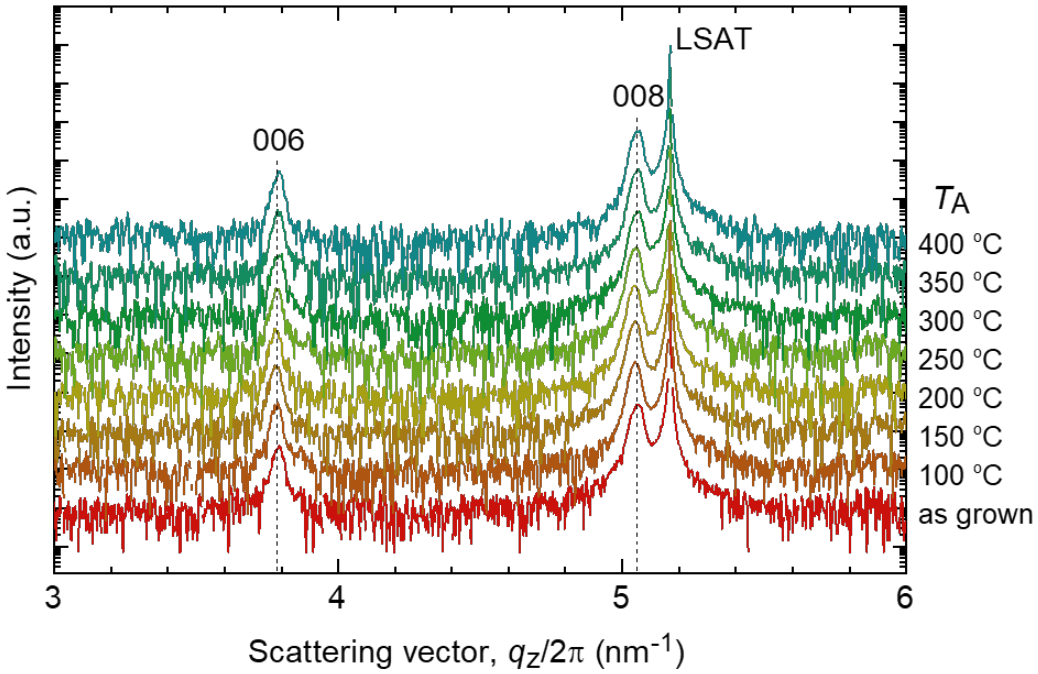

Figure S9. Out-of-plane XRD patterns of the $SrCoO_{2.5}$ films annealed at several temperatures in air. Note these XRD patterns were measured at room temperature in air. The peak position and intensity of both 006 and 008 BM-$SrCoO_{2.5}$ did not change after the annealing.

Table S1. Representative values of the thermopower and the resistivity of the $SrCoO_{2.5}$ film annealed at several temperatures in air. Note that the values were measured at room temperature in air.

Annealing temperature, T_A (°C)	Thermopower, S (μV K^{-1})	Resistivity, ρ (Ω cm)
as grown	+126	10.3
200	−207	9.7
300	−147	28.6
400	+136	18.7